Deformation of Rubber-Toughened Polycarbonate: Macroscale Analysis of the Damage Zone

CHIHMIN CHENG,[1] A. HILTNER,[1,*] E. BAER,[1] P. R. SOSKEY,[2] and S. G. MYLONAKIS[2]

[1]Department of Macromolecular Science and Center for Applied Polymer Research, Case Western Reserve University, Cleveland, Ohio 44106; [2]EniChem America Inc., Research and Development Center, 2000 Cornwall Rd., Monmouth Junction, New Jersey 08852

SYNOPSIS

Two commercial core–shell rubbers were used as impact modifiers for polycarbonate (PC). Specimens with a single semicircular edge notch were stretched uniaxially in order to study the prefracture damage evolution of blends under a triaxial tensile stress state. The irreversible deformation of modified PC included a cavitation mechanism in addition to the three shear modes of unmodified PC. At the macroscopic level, the cavitation condition could be described by a mean stress concept. The corresponding critical volume strain for cavitation in PC blends was determined to be independent of rubber content but differed for the two impact modifiers. The critical volume strain for cavitation was used as an index of cavitation resistance for the impact modifiers. The effect of rubber content and temperature on Izod impact strength of the PC blends was also reported. From the relationship between the cavitation resistance and the Izod impact strength, it was proposed that impact modifiers with a higher cavitation resistance impart better toughness to blends with PC. © 1994 John Wiley & Sons, Inc.

INTRODUCTION

Polycarbonate (PC) is considered a tough polymer when compared to other unmodified systems such as nylon or thermoplastic polyesters. However, its application is limited by the solvent sensitivity and by notch sensitivity in thicker samples and at lower temperatures. Consequently, the addition of low levels of impact modifiers is desirable to provide extra toughness for demanding applications. Various polymers have been used to toughen PC, including polyolefins,[1,2] ABS,[3,4] styrenic block copolymers,[5] and core–shell rubbers.[6–10]

The composite nature of core–shell rubbers is quite attractive in impact modification of plastics. In principle, the rubbery core provides resistance to impact, especially at lower temperature, whereas the grafted glassy shell provides rigidity and compatibility to the matrix that ensures the desired particle shape and good dispersion. Therefore, the control

of processing conditions is not as critical as with other impact modifiers such as ABS[3,4] and SBS elastomer.[5] In addition, the versatility of emulsion polymerization provides a level of control on the particle composition, morphology, and size so that the core–shell parameters can be modified to match the requirements for impact performance.

Impact testing is one of the most popular ways to evaluate rubber-toughened polymers. Izod impact test results provide information for comparing the toughening efficiencies of different impact modifiers. However, the origin of the differences in toughening behavior are not apparent. To design an effective impact modifier, the deformation mechanisms must be understood.

Unmodified PC deforms by pure shearing. The modes of shear yielding in PC under the triaxial stress state produced at a semicircular edge notch by uniaxial loading have been characterized.[11] Core yielding consists of two families of shear flow lines, called slip lines, that grow out of the notch root in the center of the specimen where the triaxial stress is highest. Growth of the core yielding zone is constrained by the surrounding elastic material. The

triaxial stress concentration at the plastic–elastic boundary can lead to failure. For example, in thick glassy polymers, the plastic–elastic boundary is the site of catastrophic crack initiation.[12] Core yielding may also be followed by two modes of through-thickness global yielding, the plane stress intersecting shear mode in thinner specimens or the plane strain hinge shear mode in thicker specimens.

The addition of a rubbery phase to the PC matrix introduces the possibility of cavitational mechanisms and, as a result, competition and interaction of cavitation and shearing processes. A previous study of the toughening mechanisms in sharp-notched specimens of PC blended with core–shell rubber suggested that cavitation of rubber particles occurred first, followed by shear yielding of the matrix polymer.[7]

Cavitation is recognized as an effective mechanism for toughness enhancement because it relieves the hydrostatic strain energy and enhances shear deformation in the matrix.[13] Rubber particles lose their toughening function in an epoxy matrix when cavitation is suppressed by an imposed hydrostatic pressure.[14] Cavitation of a rubber particle in a blend is controlled by the nature and the degree of cross-linking of the core component, the interfacial adhesion with the matrix, and the stress state. To understand impact enhancement, it is useful to examine the cavitation behavior of impact modifiers in a matrix under a triaxial stress state.

The cavitation behavior of PVC and transparent PVC/rubber blends has been quantitatively studied by examining the stress-whitened damage zone that forms at a blunt notch. The blunt notch geometry was used to create a triaxial stress state while minimizing the tendency for crack growth.[11,13,15–17] An elastic analysis of the prefracture damage zone provided a critical volume strain for cavitation that was independent of blend composition and temperature. Similar results were obtained using transparent PVC/MBS blends.[17]

In this study, the deformation of PC modified with two core–shell rubbers was investigated. Using the previous methodology,[15] the damage zone that formed ahead of a blunt notch was analyzed to obtain the cavitation condition. The relationship between the cavitation resistance of PC/rubber blends and Izod impact strength was then examined.

EXPERIMENTAL

Materials

The matrix polymer was a commercial polycarbonate (PC), produced by EniChem SpA, designated

as Sinvet 251, with a molecular weight of around 32,000. Two commercial MBS impact modifiers were used: Paraloid EXL-3607 (PL) rubber from Rohm and Haas Co. and Metablen E-900 (MB) rubber manufactured by AtoChem North America Inc. The monodisperse PL particles were 0.2 μm in diameter. The particle-size distribution of MB rubber was bimodal with large and small particles of 0.34 and 0.08 μm. The large particles constituted more than 90% of the total rubber. The glass transition temperature of PC was 150°C and the glass transition temperature of both rubbers was −70°C measured at 1 Hz by DMTA (Polymer Laboratories).

Blending

The starting materials were dried at 125°C for 15 h in a forced-air oven. The dry pellets were premixed by hand and placed in the covered feed hopper of the mixing extruder with a blanket of nitrogen gas. A 34 mm Leistritz twin-screw corotating extruder was used to prepare the blends. This extruder has a modular barrel and screw design for a flexible setup. A series of kneading disks were used along the screw profile to ensure good distributive mixing of the modifiers throughout the blend. A vacuum section was placed in the extruder barrel near the die exit to remove any residual moisture or volatile components. The melted blend was extruded through a two-hole die plate. The resulted strand was fed through a water bath and pelletized. Typical operating conditions for the extrusion blending were 250°C barrel temperature, 150 rpm screw speed, 15 kg/h feed rate, 7.5 kw drive power, 260°C melt temperature, and −900 mbar vacuum port.

The blend pellets were dried again before test pieces were injection-molded. An 80 ton NISSEI injection-molding machine was used to produce tensile and impact specimens. Typical operating conditions for the molding were 265°C barrel temperature, 265°C nozzle temperature, 96°C mold temperature, 14,000 psi injection pressure, and 10,000 psi hold pressure.

Mechanical Testing

An Instron Model 1123 machine was used for mechanical tests. The uniaxial tensile tests were performed on 3.18 mm-thick injection-molded ASTM D638 tensile specimens with three crosshead speeds (0.1, 1, and 10 mm/min). The Young's modulus and yield stress were obtained from tensile tests at ambient temperature with an extensometer to measure strain. The crosshead speed of 10 mm/min provided a strain rate equivalent to the effective strain rate at the notch root when notched specimens were

tested under the conditions described below.[18] A 1 mm radius semicircular notch was machined with an end mill midway along one edge of 3.18 mm-thick tensile specimens. The notched specimens were mounted in an Instron machine with 115 mm separating the grips. Tensile tests were performed at ambient temperature with a crosshead speed of 0.1 mm/min. Specimens of PC and blends with 1 and 2% rubber were sufficiently transparent that the damage zone could be photographed during loading with a traveling microscope in the transmission mode at a magnification of 20×. Due to the opacity of blends with 3% or more rubber, specimens were stretched to the desired stress level and sectioned after unloading in order to view the damage zone. The midplane of the damage zone was cut into approximately 0.3 mm-thick sections with a low-speed, water-cooled Isomet saw. The sections were viewed with an Olympus Model BH2 optical microscope in the transmission mode.

A Tinius Olsen pendulum impact testing machine with a low-temperature unit was used to perform all the impact tests. Notched Izod specimens 3.18 and 6.35 mm thick were prepared and tested according to ASTM D256 specifications.

Electron Microscopy

Sections for transmission electron microscopy (TEM) were prepared by embedding the specimen in epoxy followed by trimming and staining for 3 days in a 2% aqueous solution of osmium tetroxide. After staining, sections were wet cryo-microtomed with an RMC MT6000-XL ultramicrotome with a CR-2000 cryo-sectioning unit. Temperatures were −90°C for the specimen and −50°C for the diamond knife. A mixture of water and DMSO was used as the trough fluid. The sectioning direction was parallel to the injection direction. The 80–130 nm-thick sections were examined in a JEOL 100SX transmission electron microscope.

Fracture surfaces of the impacted specimens were examined in the scanning electron microscope. The specimens were sputter-coated with a thin layer of Au/Pd and examined in a JEOL 840A scanning electron microscope.

RESULTS AND DISCUSSION

Tensile Properties of Unnotched Specimens

The engineering stress–strain curves of PC and PC blends are shown in Figure 1. Both unmodified and modified PC exhibited a yield maximum that was accompanied by the formation of a neck, followed by cold drawing and strain hardening. Visually, no difference in the shape of the neck profile of PC and the blends could be discerned. Blends with less than 3% rubber were translucent and did not exhibit obvious stress-whitening after yielding. The uniaxial tensile properties of PC blends measured with a crosshead speed of 10 mm/min are tabulated in Table I; PL blends and MB blends possessed very similar tensile properties.

The dependence of the Young's modulus (E) on rubber content at room temperature is shown in Figure 2. Experimental results were lower than pre-
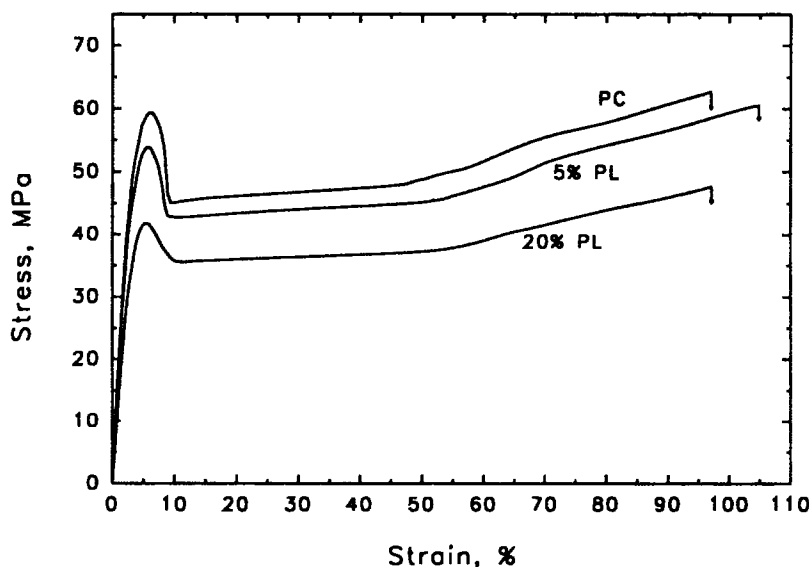

Figure 1   Engineering stress–strain curves of PC and PC blends.

Table I   Mechanical Properties of PC/rubber Blends[a]

Materials	Young's Modulus E (GPa)	Stress at Yield σ_y (MPa)	E/σ_y	Strain at Yield (%)	Stress at Break (MPa)	Strain[b] at Break (%)	Index of Cold Drawing σ_y/σ_d[c]
PC	2.50	59.8	41.8	6.5	64.3	103	1.28
1% PL	2.41	58.9	41.1	6.5	66.5	115	1.28
2% PL	2.39	58.0	41.2	6.4	66.2	104	1.27
3% PL	2.30	57.5	40.0	6.5	63.6	102	1.27
5% PL	2.21	54.2	40.4	6.1	58.5	99	1.24
10% PL	2.07	51.0	40.2	6.1	56.6	102	1.21
20% PL	1.70	42.2	40.3	5.6	46.6	90	1.13
1% MB	2.42	59.8	40.5	6.4	65.2	92	1.29
3% MB	2.34	57.7	40.5	6.2	62.9	101	1.28
5% MB	2.29	54.9	41.7	5.8	57.9	95	1.26
10% MB	2.17	53.2	40.7	6.0	51.3	75	1.23

[a] ASTM D638, crosshead speed: 10 mm/min.
[b] Standard deviation is within 20%, gauge length: 95 mm.
[c] σ_y: upper yield stress; σ_d: lower yield stress.

dicted by the rule of mixtures. The decrease in modulus with an increase of rubber content was satisfactorily modeled by Kerner's equation for a rubber-filled polymer and by the Lewis/Nielsen equation with a random loose-packing correction.[19]

The yield stress (σ_y) exhibited a linear decrease with rubber content as shown in Figure 3. Rubber had the same effect on the yield stress as on the modulus since the ratio of Young's modulus to yield stress (E/σ_y) was independent of the rubber content

up to 20 wt % rubber (Table I). A ratio of modulus to yield stress around 40 is typical of glassy polymers.[20]

One of the parameters used to describe the yield instability of polymeric materials is the index of cold drawing defined as the ratio of the upper yield stress (σ_y) to the lower yield stress or draw stress (σ_d). The larger the index of cold drawing, the sharper or more localized the necking. The blends exhibited a linear decrease in the index of cold drawing with
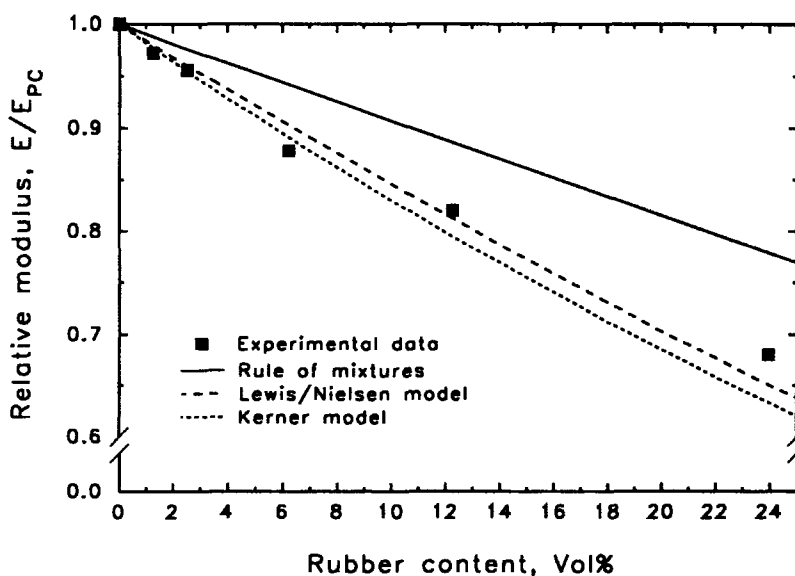

Figure 2   Dependence of Young's modulus on rubber content for PL blends.
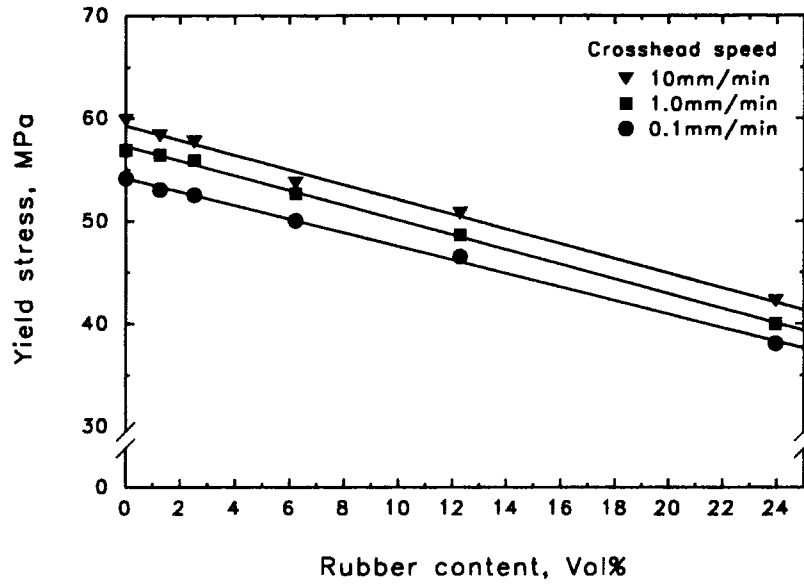
Figure 3   Dependence of yield stress on rubber content for PL blends.

increasing rubber content (Table I). This observation implied that yielding was more delocalized in the blends than in PC, even though there were no obvious differences in the neck profile.

Damage Zone

Figure 4 shows the stress-displacement curve of a 1% PL blend specimen with a semicircular notch. The notch root was photographed during deformation, and the arrows indicate the positions at which the following sequence of micrographs was taken. With the focus on the center of the specimen, core yielding was observed at position 1 on the stress-displacement curve [38.5 MPa, Fig. 5(a)] as two families of slip lines growing out from the notch. The region defined by the slip lines was designated as the core yielding zone. As the core yielding zone increased in size at position 2 [41.0 MPa, Fig. 5(b)], a dark zone appeared at the tip. This dark zone,
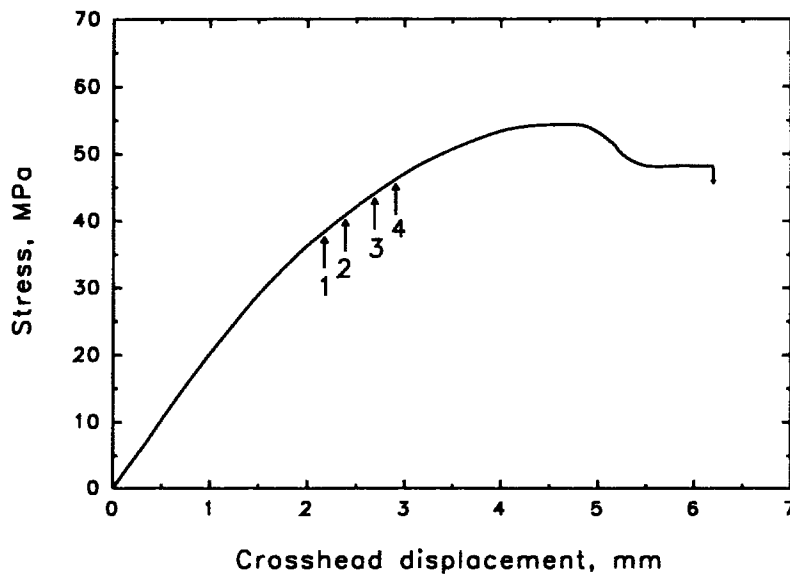

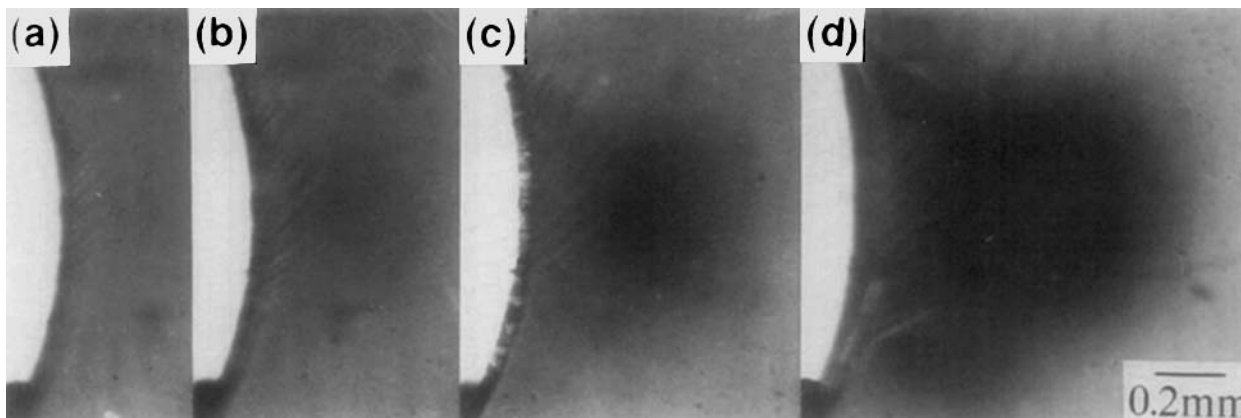**Figure 4**   Stress-displacement curve of 1% PL blend with a semicircular notch.

Figure 5   Optical micrographs of the damage zones in 1% PL blend: (a) position 1, 38.5 MPa; (b) position 2, 41.0 MPa; (c) position 3, 43.9 MPa; (d) position 4, 46.2 MPa.

which was not observed in unmodified PC, was caused by stress-whitening. Both the core yielding zone and stress-whitened zones (SWZ) continued to increase in size as the stress increased to positions 3 and 4 [Fig. 5(c) and (d)]. At higher stress levels, the same modes of global yielding were observed in the blends as in unmodified PC. The appearance of stress-whitening at the tip of the core yielding zone was the primary difference between damage zone evolution in PC and in the blends. A deformation sequence similar to that of the PC blends, with core yielding followed by appearance of a stress-whitened zone, was observed previously in PVC[15] and PVC/MBS blends.[17]

Deformation of Rubber Particles in the Stress-whitened Zone

Micrographs of the undeformed blend with 5% PL in Figure 6(a) and (b) show that the 0.2 μm monodisperse particles of the PL rubber were well dispersed in the blend. Furthermore, it was apparent that the rigidity of the particles was sufficient to prevent particle distortion by shearing during the blending process. A section from the cold-drawing region of an unnotched tensile specimen in Figure 6(c) shows that the particles were deformed along with the matrix to a draw ratio of about 1.8. Due to the low triaxiality in the neck, the particles were not cavitated. For this reason, the unnotched stress–strain behavior was not useful for comparing PC impact modifiers that exhibited cavitation as part of the toughening mechanism.

In contrast to sections from the unnotched blends, a section from the stress-whitened zone of

the notched 5% PL blend shows that the deformed particles had retained their spherical shape but had increased in size and cavitated [Fig. 6(d)]. Since light scattering from the cavitated rubber particles was the cause of stress-whitening, the boundary of the stress-whitened zone defined the region where the hydrostatic component of the stress intensification was high enough to cause particle cavitation. The fact that cavitation occurred predominantly in the particles and only occasionally at the matrix–particle interface implied good interfacial adhesion between PL particles and PC.

Core Yielding Zone

The slip lines of the core yielding zone of PC and the blend with 2% PL are compared in Figure 7. The slip lines in rubber-modified PC were thinner and more numerous when compared to those of unmodified PC. This observation was consistent with the delocalization of yielding, a phenomenon also suggested by the decrease in index of cold drawing. A primary requirement for matrix toughening is believed to be this efficient delocalization of matrix shear yielding by the impact modifier in a matrix that deforms predominantly by shearing.[21-23]

The characteristic slip-line field of the double logarithmic spirals for a pressure-dependent material is given by[15]

$$\theta \cot \psi = \pm \ln(r/a) + \text{constant} \qquad (1)$$

in polar coordinates (r, θ) with the origin at the notch center. In this equation, a is the notch radius; r, the distance from the notch origin to the tip of
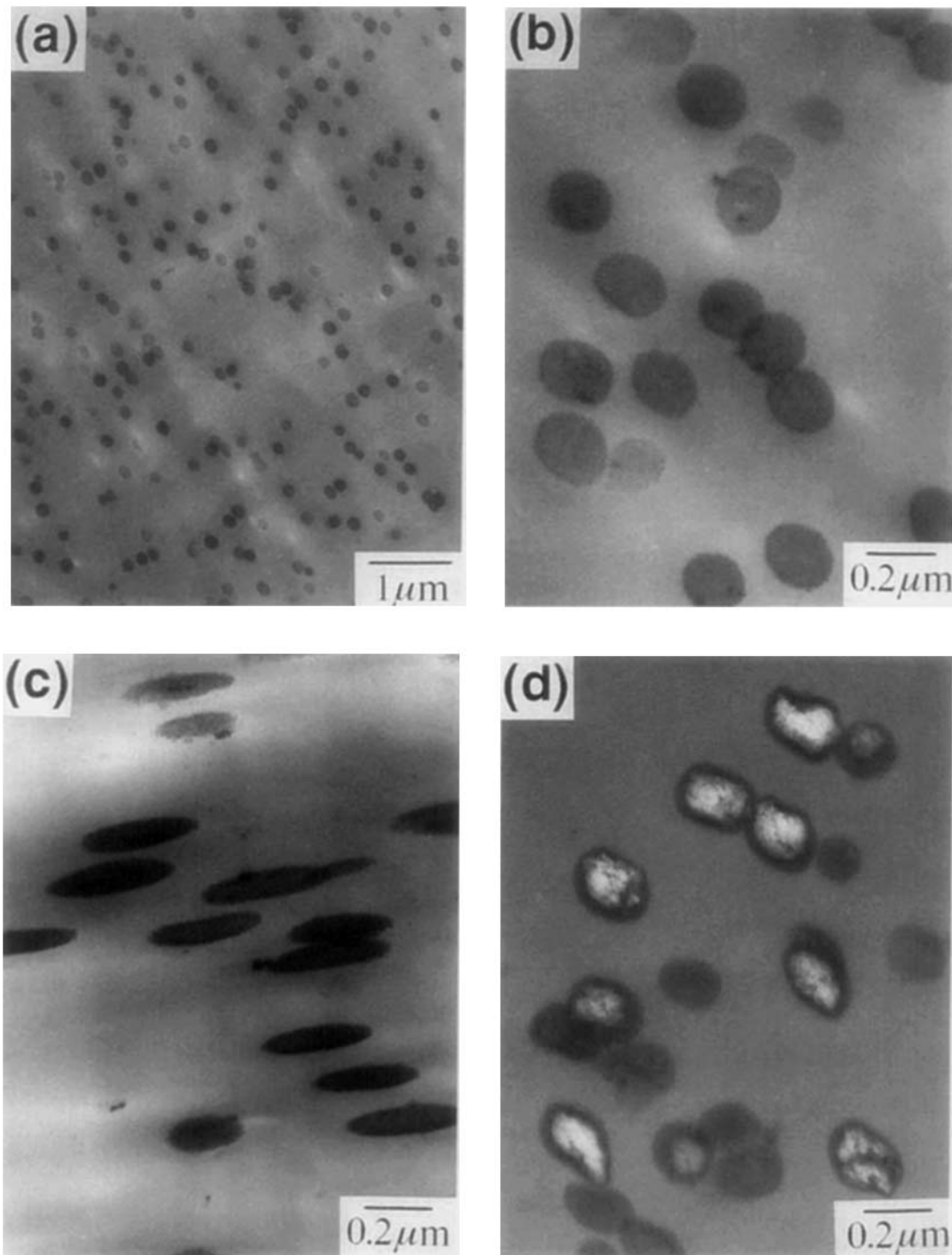
Figure 6   Transmission electron micrographs of 5% PL blend: (a, b). The undefomed blend at two magnifications; (c) the necked region of an unnotched specimen, the arrow indicates the direction of deformation; (d) the stress-whitened zone of a notched specimen.

the slip-line field; and 2ψ, the angle between slip lines and is related to the pressure-dependent coefficient, μ, in the modified von Mises yield criterion by $\mu = \cos 2\psi$. Using the published value of $\mu = 0.07$ for PC,[24] the calculated angle between α and β slip lines was 85.3°. The experimental slip-line angles
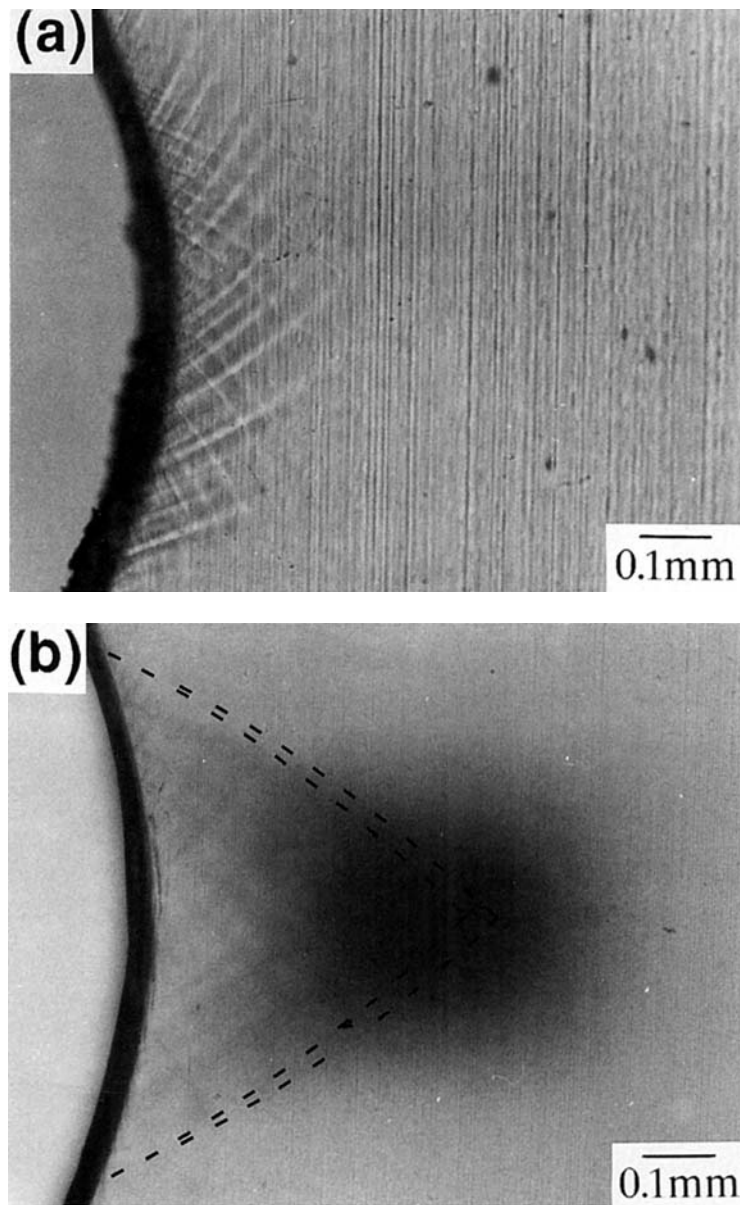
Figure 7   Optical micrographs showing slip lines at the notch root: (a) unmodified PC; (b) blend with 2% PL. The outer and inner curves were calculated from eq. (1) with and without pressure-dependent yielding modification, respectively.

of PC and the blends were similar and in the range of 84°–87°. The consistency between the calculated slip-line angle and experimental observations suggested that the PC blends followed the same pressure-dependent yield criterion as did PC. The curves in Figure 7(b) were calculated from eq. (1). The inner pair of curves was calculated without the pressure dependency ($\mu = 0$), whereas the outer pair of curves, which better paralleled the trajectories of

the slip lines, was obtained when the pressure dependency was included in the calculation.

It was possible to calculate the length of the core yielding zone from eq. (1) by using the micrographs to determine the angle θ at which the boundary of the core yielding zone intersected the notch surface. The length of the core yielding zone increased linearly with the remote stress (Fig. 8). Extrapolation gave the condition for initiation of core yielding at
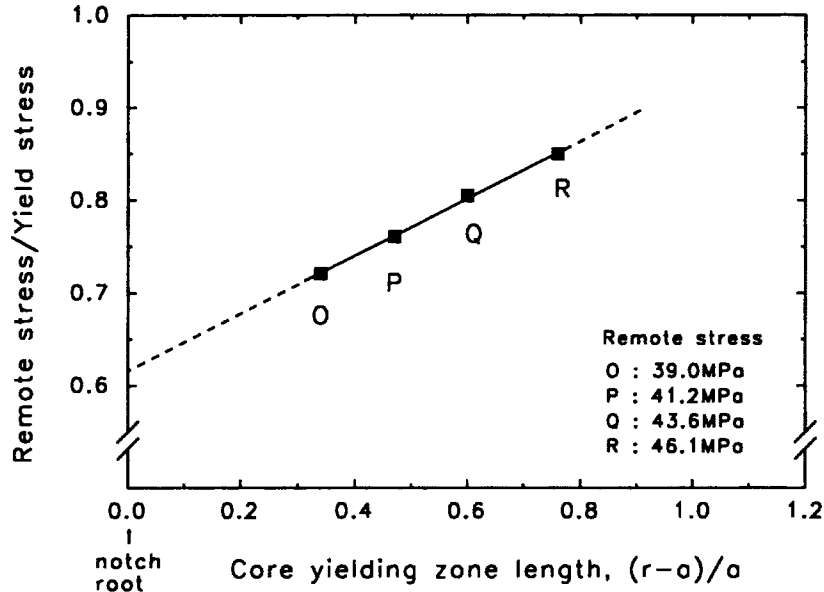
Figure 8   Length of the core yielding zone as a function of remote stress for the 5% PL blend.

the notch root to be $0.62\sigma_y$, which is close to the von Mises prediction of $0.577\sigma_y$.

Stress-whitened Zone

Contours of the SWZ in Figure 9 show the increase in size and change in shape as the remote stress increased. At low stresses, the stress-whitened zone possessed a circular shape regardless of the amount of rubber in the blend. At higher stress levels, the SWZ changed from a circular to a triangular shape. This change of shape became more pronounced as the amount of rubber increased.

The position of the SWZ on the x-axis is plotted in Figure 10 for 5% PL blend as a function of normalized stress (σ_o/σ_y). The distances from the notch root to the boundaries of the SWZ was measured directly from optical micrographs. As illustrated in Figure 10, the position of the near-notch boundary of the SWZ was relatively constant, whereas the far-notch boundary moved away from the notch as the remote stress increased. The position at which cavitation initiated was obtained by extrapolation to the point of intersection (A). Since the position of the near-notch boundary did not change as the load increased, point A, where cavitation initiated, was taken as the position of the near-notch boundary. The distance from the notch root to the near-notch boundary depended on the amount of rubber. The distance was larger for the PL blends than for the MB blends (Table II). The distance from the notch root to the near-notch boundary also increased when
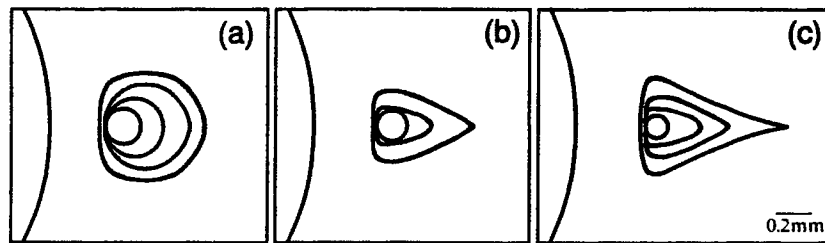

Figure 9   Contours of the stress-whitened zone in PL blends at various remote stresses: (a) 1% PL; (b) 5% PL; (c) 10% PL. For all cases, the remote stress of the outermost contour was 82% of the yield stress.
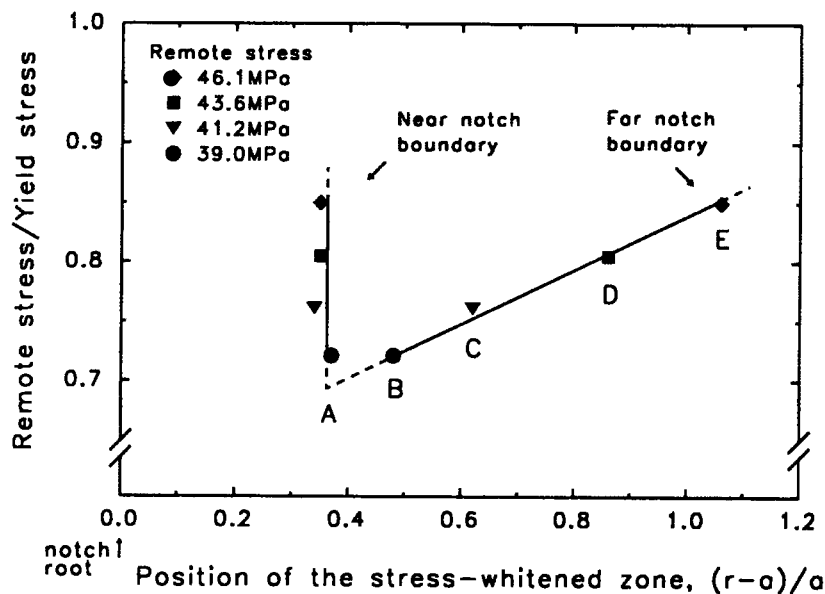
Figure 10 Growth of the stress-whitened zone in the 5% PL blend.

the amount of rubber increased from 1 to 5%, but was about the same for 5 and 10% rubber.

Analysis of the Stress-whitened Zone

The stress field at point A characterized the initiation condition of cavitation. The critical cavitation stress was calculated from the pressure-dependent slip-line field theory. The plastic stress field in the core yielding zone is schematically shown in Figure 11. The plastic stress distribution along the x-axis in the slip-line field of a pressure-dependent material for the case of a semicircular notch is given by[15]

$$\sigma_{rr} = \frac{k_0}{\mu}\left[1 - \left(\frac{r}{a}\right)^{-2\mu/(1+\mu)}\right] \qquad (2)$$

$$\sigma_{\theta\theta} = \frac{k_0}{\mu}\left[1 - \left(\frac{1-\mu}{1+\mu}\right)\left(\frac{r}{a}\right)^{-2\mu/(1+\mu)}\right] \qquad (3)$$

Table II   Cavitation Condition at Near-Notch Region of the Stress-Whitened Zone for PC/Rubber and PVC/Rubber Blends

Rubber Content	Near-Notch Boundary (mm)	Yield Stress[a] σ_y (MPa)	Critical Mean Stress σ_{mc} (MPa)	Young's Modulus[a] E (MPa)	Critical Volume Strain V_c (%)
1% PL	0.27	58.9	44.6	2410	1.44
5% PL	0.36	54.2	44.7	2210	1.57
10% PL	0.35	51.0	41.7	2070	1.57
1% MB	0.16	59.8	40.1	2420	1.29
5% MB	0.23	54.9	39.9	2290	1.36
10% MB	0.24	53.2	39.1	2170	1.40
PVC[b]	0.11	68.7	42.5	3700	0.8
PVC/MBS[c]	0.06	57.1	32.8	3100	0.8

[a] Crosshead speed: 10 mm/min.
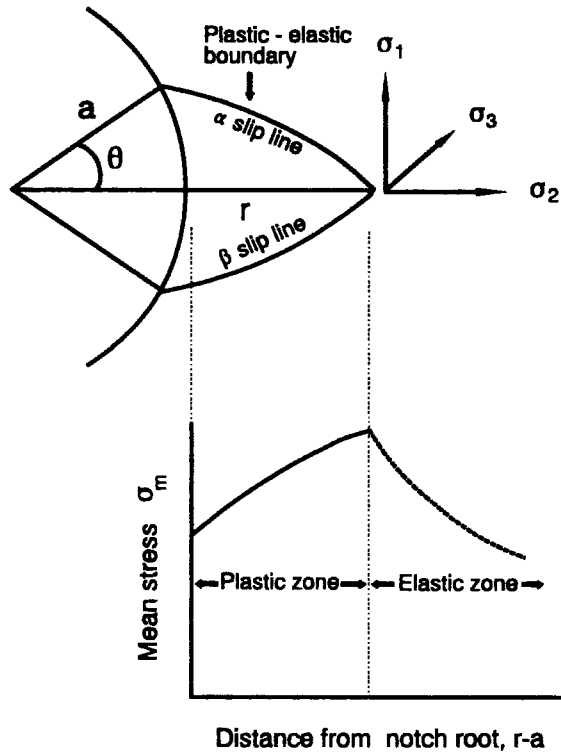[b] Ref. 15.
[c] Blend contains 5% MBS. Ref. 17.

Figure 11 Stress field in the core yielding zone from slip-line field theory.

$$\sigma_{r\theta} = 0 \qquad (4)$$

where σ_{rr} and $\sigma_{\theta\theta}$ are the normal stresses; $\sigma_{r\theta}$, the shear stress; k_0, the shear yield stress; μ, the pressure-dependent coefficient of PC; a, notch radius; and r, the distance from the tip of the core yielding zone to the notch origin. The stress concentration at the plastic–elastic boundary increases with the length of the core-yielding zone. As the core yielding zone lengthens with increasing remote stress, the stress concentration at the tip increases until the stress at the plastic–elastic boundary is high enough to cause cavitation. The position of the zone tip when the stress concentration is high enough to cause cavitation is identified as point A in Figure 10. Since A coincides with the near-notch boundary of the SWZ, it is possible to compare the cavitation resistance of different rubbers using the distance from the notch root to the near-notch boundary. The further the boundary is from the notch root, the higher the stresses required for cavitation, or the higher the cavitation resistance of the rubber.

Cavitation is often described by a mean stress criterion defined as $\sigma_m = (\sigma_{rr} + \sigma_{\theta\theta} + \sigma_{zz})/3$. The

mean stress in the plastic zone assuming plane strain ($\sigma_{zz} = \nu(\sigma_{rr} + \sigma_{\theta\theta})$) is given by

$$\sigma_m = \frac{k_0}{\mu}\left[1 - \left(\frac{1}{1+\mu}\right)\left(\frac{r}{a}\right)^{-2\mu/(1+\mu)}\right] \qquad (5)$$

The corresponding volume strain is given by

$$V_c = \frac{3(1 - 2\nu)\sigma_m}{E} \qquad (6)$$

where E is Young's modulus. The cavitation condition calculated for PL and MB blends is tabulated in Table II. The calculated critical mean stress for cavitation was in the range of 42–45 MPa for PL blends and 39–40 MPa for MB blends. The effective cavitational strength of polybutadiene at room temperature is estimated to be 30–40 MPa.[25]

The critical volume strain of cavitation calculated from eq. (6) showed little dependence on rubber content (Table II); the value was about 1.50% for PL blends. This observation implied that the onset of cavitation was not strongly influenced by the stress fields induced by neighboring particles. Similar results regarding the independence of the critical volume strain of cavitation on rubber content were found in PVC/CPE blends[16] and PVC/MBS blends[17] and also in a study of nylon toughened with EPDM where the initiation strain of cavitation was measured by tensile dilatometry.[26]

To describe the growth of the SWZ with increasing remote stress, it was assumed that the material stress-whitened only if the local stress was higher than the critical mean stress of cavitation. The schematic drawing of the redistributed mean stress distribution along the x-axis ahead of the notch in Figure 11 follows a concept developed previously to describe growth of the SWZ in PVC.[15] Beginning at the notch root, the mean stress along the x-axis first increases due to the presence of the core yielding zone. The maximum in the curve indicates the position of the plastic–elastic boundary; the mean stress then decreases following a redistributed elastic curve. The boundaries of the SWZ on the x-axis and the mean stress distribution in the damage zone are plotted together in Figure 12. Position A is the initiation point of cavitation determined by the near-notch boundary of the SWZ. The mean stress at this point was identified as the critical mean stress of cavitation. The plastic–elastic boundary at higher remote stresses, positions O, P, Q, and R, was calculated from eq. (1). Positions B, C, D, and E locate the far notch boundary of the SWZ at remote stresses of 39.0, 41.2, 43.6, and 46.1 MPa, respec-
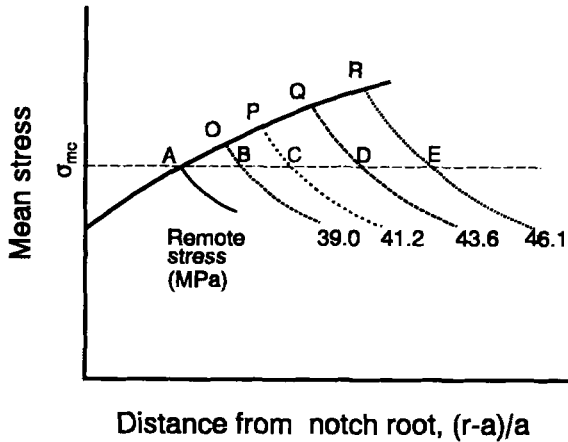
Figure 12 Stress distribution ahead of the semicircular notch that accompanies growth of the stress-whitened zone.

tively. The region where the mean stress is higher than the critical mean stress for cavitation corresponds to the region that showed stress-whitening. At a remote stress of 39.0 MPa, the mean stress profile in the stress-whitened zone followed curve AOB. The stress distribution in the SWZ at other remote stresses can be similarly described.

The stress-displacement curves of notched specimens were identical for PL and MB blends with the same rubber content. However, the differences in the SWZ were distinguishable as shown in Figure 13 where the damage zones are compared at the same stress levels. Initiation of the SWZ occurred at a lower stress in the MB blend, and the near-notch boundary was located closer to the notch. The cavitation condition of MB blends is also included in Table II. Because the distance to the near-notch
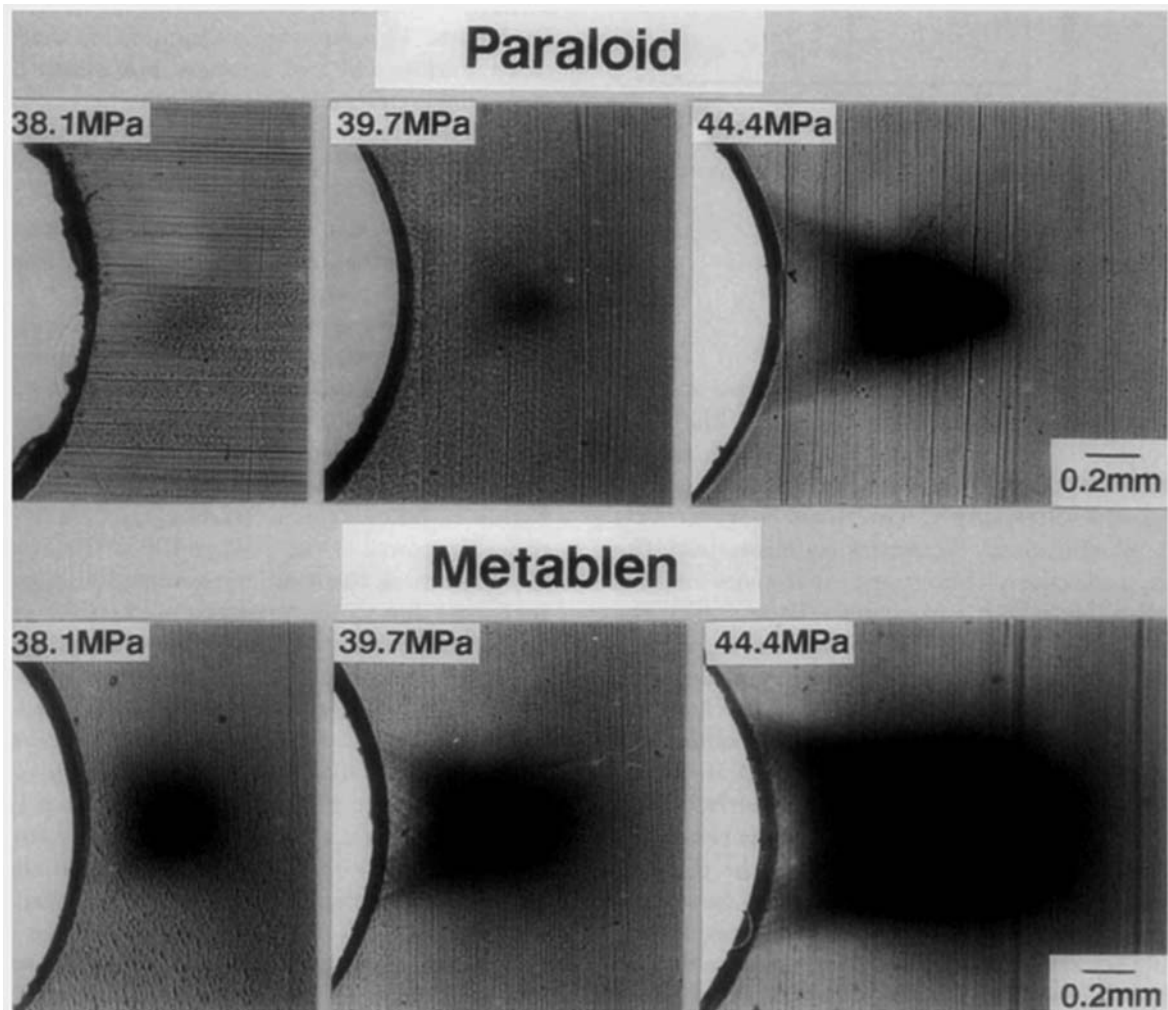

Figure 13 Optical micrographs comparing the stress-whitened zone of 5% PL blend and 5% MB blend at three stresses.

boundary was shorter in the MB blends than in the PL blends, the critical mean stress of cavitation was slightly smaller, as was also the critical volume strain of cavitation (1.35% compared to 1.50%). The critical volume strain is a measure of the resistance to cavitation; the cavitation resistance of PL blends was slightly greater than that of MB blends.

Impact Properties

The Izod impact strength was measured for PC blends modified with PL and MB rubber at a rubber content ranging from 0 to 20% and temperatures ranging from 25 to −40°C. Two thicknesses were examined, 3.18 mm (0.125 in.) and 6.35 mm (0.250 in.). The results are presented in Table III for PL blends and in Table IV for MB blends. The data showed that the ambient temperature Izod impact of the thinner sections modified with PL was unaffected by the amount of modifier up to 2%, then it decreased gradually at higher rubber loadings. The same trend was observed for MB blends. Thinner sections of the MB blends were also tested at several temperatures below ambient. The Izod impact of 3.18 mm-thick PC decreased only slightly when the temperature was lowered from 25 to −20°C, then decreased sharply between −20 and −40°C. The −40°C impact was improved dramatically by the addition of 3% MB.

Table III Effect of Test Temperature and Rubber Content on Izod Impact Strength of PC/Paraloid Blends

Rubber Content (%)	Impact Strength (J/m)			
	25°C	0°C	−20°C	−40°C
Thickness: 3.18 mm				
0	918	—	—	—
1	849	—	—	—
2	860	—	—	—
3	812	—	—	—
4	785	—	—	—
5	785	—	—	—
10	651	—	—	—
20	336	—	—	—
Thickness: 6.35 mm				
0	112	134	128	112
1	454	224	123	134
2	870	267	219	192
3	886	812	230	214
4	844	801	689	331
5	801	764	662	283
10	700	614	555	427
20	555	422	395	336

Table IV Effect of Test Temperature and Rubber Content on Izod Impact Strength of PC/Metablen Blends

Rubber Content (%)	Impact Strength (J/m)			
	25°C	0°C	−20°C	−40°C
Thickness: 3.18 mm				
0	886	849	833	117
1	918	812	790	459
3	828	801	758	673
5	812	737	694	582
10	683	700	657	571
Thickness: 6.35 mm				
0	107	134	128	144
1	166	134	171	128
3	828	689	203	198
5	764	657	347	267
10	700	587	422	294

The large drop in the 25°C impact of PC from 918 to 112 (J/m) when the thickness was increased from 3.18 to 6.35 mm was characteristic of a ductile-to-brittle transition and demonstrated the profound sensitivity of PC to the triaxial stress state (Table III). Blending 2% PL or 3% MB with the PC increased the 25°C impact to values comparable to those obtained with thinner PC specimens. The dependence of the 25°C impact on the amount of PL rubber in Figure 14 shows that the ductile-to-brittle transition occurred with 2% PL and that the highest impact was achieved with 3% PL. Although sections with more than 3% PL were also ductile, the impact decreased gradually with increasing PL due primarily to the decreasing yield strength. The amount of PL required to produce ductility increased as the temperature decreased. Thus, 3% PL was required at 0°C and 4% PL at −20°C. No sharp increase in impact was observed at −40°C; instead, the impact increased gradually up to 10% PL.

The data in Table III and Figure 14 also show the effect of PL on the ductile-to-brittle transition temperature (DBTT). The DBTT of 6.35 mm sections dropped from above room temperature for PC to around −30°C with 4–5% PL. When the PL was increased to 10 and 20%, the blend appeared to lose the ductile-to-brittle transition. The impact was almost independent of temperature, but the absolute values were lower than the ductile impact values of blends with lower amounts of PL.

The effect of MB on the DBTT of 6.35 mm specimens is shown in Figure 15. Although the features are similar to those observed for PL blends, MB did
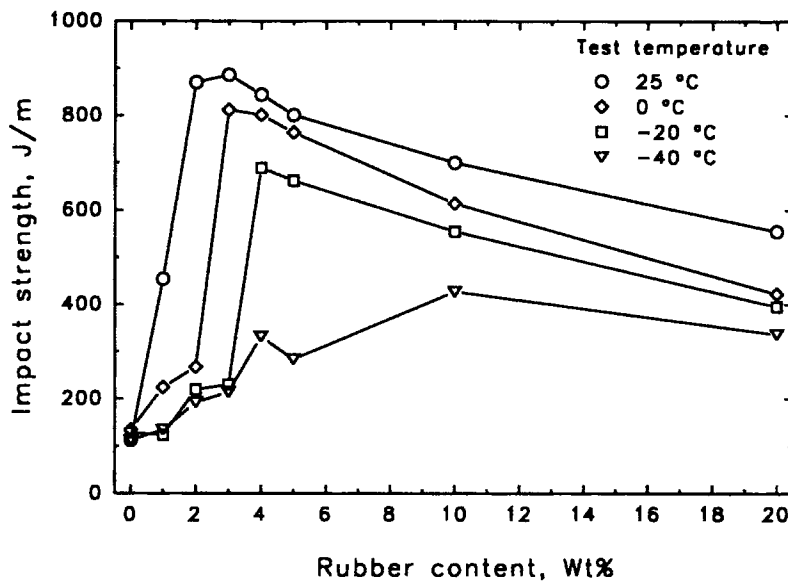
Figure 14 Effect of rubber content on the Izod impact strength of 6.35 mm-thick PL blends at various temperatures.

not appear to be as effective as the PL in dropping the DBTT. Whereas the PL blends showed a sharp DBTT at about −30°C with 5% rubber content, blends with MB showed a broad DBTT at about −10°C with lower impact values before and after the transition. The difference in the behavior of PL and MB may have been due to many factors including differences in particle size and particle-size dis-

tribution, interfacial adhesion with the PC, and the nature and degree of cross-linking of the core material of the particles.

The fracture surfaces of a typical low impact brittle specimen and a ductile specimen are compared in Figure 16. The brittle fracture surface of the 2% PL blend at −20°C showed the typical craze breakdown pattern that has been described in the
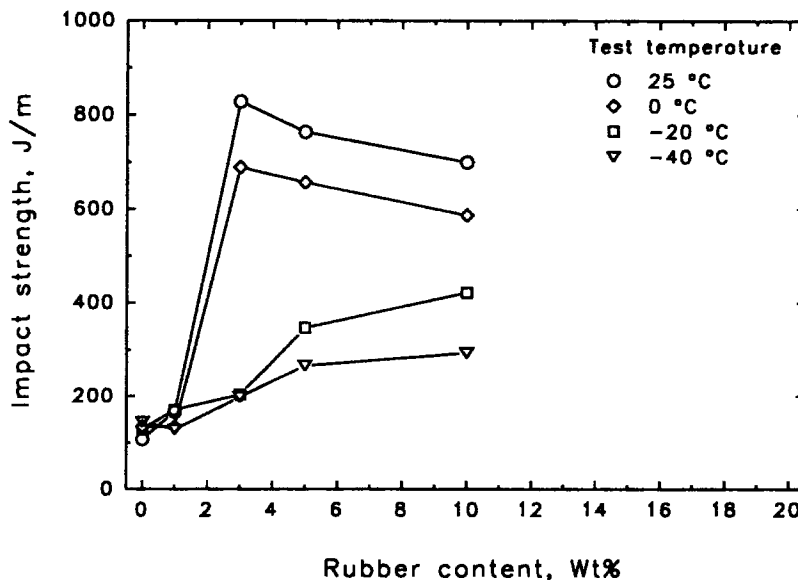

Figure 15 Effect of rubber content on the Izod impact strength of 6.35 mm-thick MB blends at various temperatures.
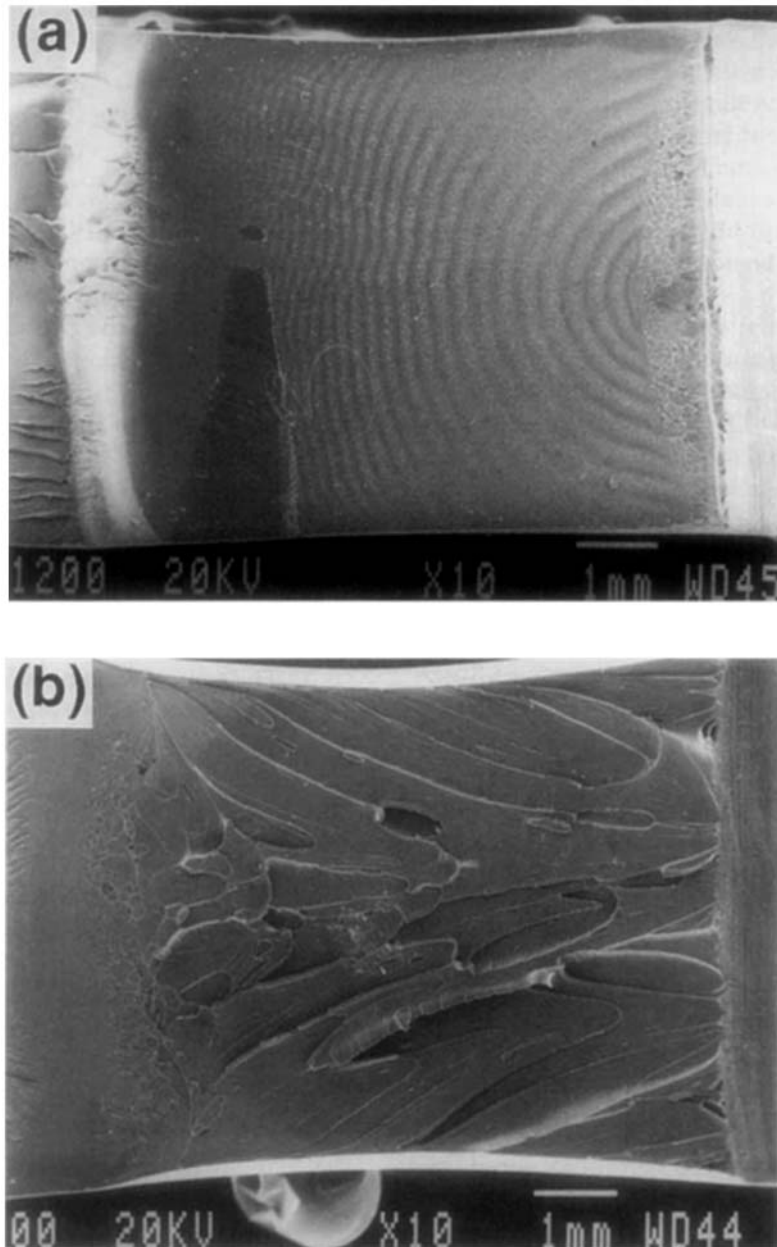
Figure 16 Scanning electron micrographs of fracture surfaces of −20°C Izod impact specimens: (a) 2% PL blend; (b) 5% PL blend.

literature,[27] with a mirror region closest to the notch followed by the mackerel and hackle regions. In comparison, the fracture surface of the 5% PL blend at −20°C was visibly stress-whitened. In low-magnification scanning electron micrographs, tear lines with characteristic sucking-in of the edges were indicative of plane stress shear fracture. At higher magnification, voids on the size scale of 0.2–0.4 μm were seen; the void density decreased with decreasing temperature and decreasing amount of rubber.

The micrographs of the 5% PL blend also revealed the furrow texture that may be associated with enhanced toughness of PC blends.[6]

Relationship of Cavitation Condition to Impact

Cavitation is thought to enhance toughness by relieving hydrostatic strain energy and promoting shear deformation of the matrix.[14] It has been postulated that a higher cavitation resistance enhances

the toughening effect.[13] Results of this investigation tend to support this argument by demonstrating a correlation between cavitation resistance of the rubber in the blend and impact strength. Although the impact improvement in thick sections at 25°C was very similar for PL and MB blends, blends with PL, the rubber with the higher cavitation resistance, had a lower DBTT and higher impact strength at low temperature than blends with the same amount of MB.

The role of cavitation resistance can be understood by considering again the stress distribution in the core yielding zone that forms at the notch root in thick PC specimens (Fig. 17). Without impact modification, the triaxial stress concentration at the plastic–elastic boundary leads to failure by formation of an internal craze and subsequent catastrophic brittle fracture. The mean stress condition at the plastic–elastic boundary for formation of a critical craze in PC has been determined to be 70–75 MPa (Ref. 12) and is indicated on the stress-distribution curve of PC in Figure 17. By blending PC with rubber particles that cavitate at a lower stress than the crazing stress of PC, the triaxiality is relieved and crazing with subsequent brittle fracture is prevented. The cavitation condition of PL and MB rubbers are indicated on the stress-distribution curve of the PC blend. Since the critical stress for rubber cavitation is lower than the crazing stress, rubber cavitation relieves the triaxiality and brittle fracture is prevented. The optimum impact modifier would then be one with a higher cavitation stress, to increase the energy absorbed by cavitation, but with a cavi-
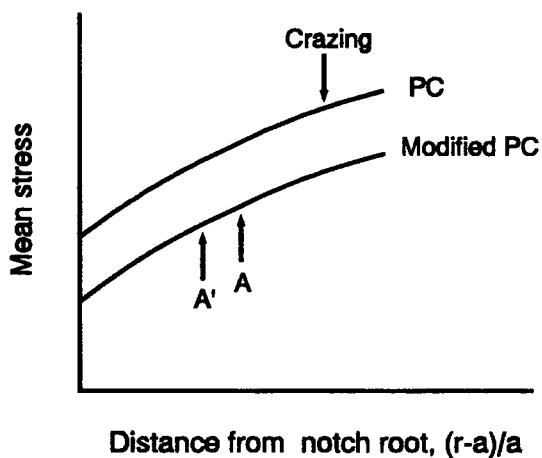
tation stress that is still well below the crazing stress of PC.

CONCLUSIONS

Analysis of the damage zone that formed ahead of a semicircular notch in PC blends during slow tensile loading provided the opportunity to assess quantitatively the cavitation resistance of two impact modifiers, Paraloid and Metablen. The study led to the following conclusions:

1. In addition to the three shear modes of deformation of PC, blends exhibit an additional mechanism, namely, stress-whitening, that appears immediately after core yielding.
2. Paraloid exhibits good interfacial adhesion in blends with PC. Stress-whitening is primarily due to cavitation in the rubber particles.
3. The critical volume strain of cavitation (V_c) in polycarbonate blends is independent of the amount of rubber but differs for the two impact modifiers that were studied. Paraloid blends have a slightly greater cavitation resistance $(V_c = 1.50\%)$ than Metablen blends $(V_c = 1.35\%)$.
4. The lower ductile-to-brittle transition temperature of Paraloid blends when compared to Metablen blends with the same amount of rubber is attributed at least in part to the higher cavitation resistance of Paraloid blends.

Figure 17   Schematic illustration of the stress distribution ahead of a semicircular notch indicating the initiation conditions for crazing in PC and rubber cavitation in (A) PL blends and (A') MB blends.

REFERENCES

1. M. A. Maxwell and A. F. Yee, *Polym. Eng. Sci.,* **21,** 205 (1981).
2. A. F. Yee, *J. Mater. Sci.,* **12,** 757 (1977).
3. M.-P. Lee, A. Hiltner, and E. Baer, *Polymer,* **33,** 675, 685 (1992).
4. M. Ishikawa and I. Chiba, *Polymer,* **31,** 1232 (1990).
5. D. W. Gilmore and M. J. Modic, *Plast. Eng.,* **April,** 51 (1989).
6. C. K. Riew and R. W. Smith, in *Rubber-Toughened Plastics,* C. K. Riew, Ed., Advances in Chemistry 222, American Chemical Society, Washington, DC, 1989.
7. D. S. Parker, H.-J. Sue, J. Huang, and A. F. Yee, *Polymer,* **31,** 2268 (1990).

8. F.-C. Chang, J.-S. Wu, and L.-H. Chu, *J. Appl. Polym. Sci.*, **44**, 491 (1992).

9. T. W. Cheng, H. Keskkula, and D. R. Paul, *J. Appl. Polym. Sci.*, **45**, 531 (1992).

10. C. Cheng, A. Hiltner, and E. Baer, *SPE, ANTEC, Conf. Proc.*, **38**, 832 (1992).

11. M. Ma, K. Vijayan, J. Im, A. Hiltner, and E. Baer, *J. Mater. Sci.*, **24**, 2687 (1989).

12. M. Ishikawa, I. Narisawa, and H. Ogawa, *J. Polym. Sci. Polym. Phys. Ed.*, **15**, 1791 (1977).

13. R. A. Pearson and A. F. Yee, *J. Mater. Sci.*, **26**, 3828 (1991).

14. D. Li, A. F. Yee, and K. Takahashi, *SPE ANTEC Conf. Proc.*, **38**, 1677 (1992).

15. A. Tse, E. Shin, A. Hiltner, and E. Baer, *J. Mater. Sci.*, **26**, 5374 (1991).

16. A. Tse, E. Shin, A. Hiltner, and E. Baer, *J. Mater. Sci.*, **26**, 2838 (1991).

17. S. Bensason, A. Tse, A. Hiltner, and E. Baer, to appear.

18. J. F. Knott and A. H. Cottrell, *J. Iron Steel Inst.*, **201**, 249 (1963).

19. L. E. Nielsen, *Mechanical Properties of Polymers and Composites*, Marcel Dekker, New York, 1981, Vol. 2.

20. N. Brown, *Mater. Sci. Eng.*, **8**, 69 (1971).

21. C. C. Chau and J. C. M. Li, *J. Mater. Sci.*, **17**, 652 (1982).

22. D. Li, X. Li, and A. F. Yee, *Polym. Mater. Sci. Eng.*, **63**, 296 (1990).

23. A. P. Berzinis, in *Thermoplastic Polymer Additives, Theory and Practice*, J. T. Lutz, Jr., Ed., Marcel Dekker, New York, 1989.

24. A. W. Christiansen, E. Baer, and S. V. Radcliffe, *Philos. Mag.*, **24**, 451 (1971).

25. A. S. Argon, R. E. Cohen, O. S. Gebizlioglu, and C. E. Schwier, in *Advances in Polymer Science, 52/53*, H. H. Kausch Ed., Springer-Verlag, New York, 1983.

26. R. J. Borggreve, R. J. Gaymans, and H. M. Eichenwald, *Polymer*, **30**, 78 (1989).

27. D. Hull and T. Owen, *J. Polym. Sci. Polym. Phys.*, **11**, 2039 (1973).